*Acta Cryst.* (1999). B**55**, 321–326

# Synchrotron X-ray analysis of the electron density in $HoFe_2$

Victor A. Streltsov[a]* and Nobuo Ishizawa[b]

[a]*Crystallography Centre, The University of Western Australia, Nedlands 6907, Australia, and* [b]*Materials and Structures Laboratory, Tokyo Institute of Technology, 4259 Nagatsuta, Midori-Ku, Yokohama 227, Japan. E-mail: strel@crystal.uwa.edu.au*

(*Received 6 May 1998; accepted 7 December 1998*)

**Abstract**

Structure factors for a small holmium diiron $HoFe_2$ Laves crystal were measured with focused $\lambda = 0.75$ Å synchrotron X-radiation using a fast avalanche photodiode (APD) counter. The deformation electron density ($\Delta\rho$) maps are remarkable for significant excess electron density midway between the Ho atoms, which is not dissimilar to the peaks attributed to classic 'covalent bonding' in C and Si crystals. These residual electrons accumulate at the centres of the kagomé net hexagons and form, with the Fe atoms, a triangular lattice which is characterized by more stable magnetic order than the kagomé net. Similar peaks occur along the Ho–Fe and Fe–Fe contacts. These results confirm the hypothesis that 5*d* electrons of the rare-earth atoms are important in the spin-coupling mechanism for $HoFe_2$-type compounds. The 5*d* electrons are far less localized than the 4*f* electrons, and considerable 5*d*–5*d* and 5*d*–3*d* orbital overlap occurs between neighbouring atoms. Aspherical electron density near the Ho nuclei can be associated with the Ho 4*f* subshell electrons. Strong depletions of the $\Delta\rho$ near the atoms along the Ho–Ho, Ho–Fe and Fe–Fe vectors are indications of exchange repulsion. The effect of anharmonicity on the $\Delta\rho$ is insignificant.

## 1. Introduction

The cubic Laves phases $R\mathrm{Fe}_2$ ($R$ = rare earth) are archetypically significant, magnetically ordered intermetallic compounds. Members of this technologically important series serve as models for studying the coexistence of 4*f* and 3*d* magnetism in a relatively simple structure. Three types of magnetic interaction, namely Fe–Fe, *R*–*R* and Fe–*R*, between the magnetic moments of the *R* and Fe atoms in a two-sublattice model are generally considered to be present in $R\mathrm{Fe}_2$ intermetallics. Whereas the high Curie temperature $T_C$ (606 K for $HoFe_2$) is mainly determined by Fe–Fe interactions, the exchange *R*–Fe and *R*–*R* couplings are responsible for the anisotropic properties of these compounds (Gignoux & Schmitt, 1995).

The Fe–Fe interactions are direct exchange interactions between the 3*d* spins, while the *R*–*R* (4*f*–4*f*) and *R*–Fe (4*f*–3*d*) interactions are indirect. Two mechanisms of these interactions have been proposed. The indirect exchange Ruderman–Kittel–Kasuya–Yoshida (RKKY) mechanism *via* the polarization of conduction electrons by local 4*f*-conduction-electron exchange has been successfully applied to simple metals. An alternative mechanism (Campbell, 1972) postulates local 4*f*–5*d* exchange and direct 5*d*–3*d* and 5*d*–5*d* interactions; it is proposed that this more adequately characterizes the interactions in rare-earth intermetallic compounds. Based on this approach, *ab initio* density-functional calculations recently performed by Brooks and coworkers (*e.g.* Brooks, 1991; Brooks *et al.*, 1991) for $R\mathrm{Fe}_2$ compounds showed that the *R* 5*d* partial moment coupled antiparallel to the Fe 3*d* moment significantly contributes to the net magnetic moment. This results from 3*d*–5*d* mixing which transfers some charge from Fe 3*d*- to *R* 5*d*-character orbitals. The *R* 4*f* and 5*d* spins are always coupled ferromagnetically by local exchange interactions and the ferrimagnetic interaction between *R* 4*f* and Fe 3*d* spins is mediated by mixing between *R* 5*d* and Fe 3*d* states. However, these theoretical calculations did not predict the *R*–*R* 5*d*–5*d*-type orbital interactions.

Although magnetic effects are due primarily to electron spin density, charge density and spin density are related by the effect of uncompensated spins on the electron probability density. Exchange correlation between electrons occurs when atoms overlap and strongly influence density distributions. As the direct magnetic exchange interaction *via d*–*d* mixing requires orbital overlap of some kind, strong 'covalent' effects on the electron density distribution in $R\mathrm{Fe}_2$ Laves compounds are expected. Therefore, an accurate experimental determination of the electron density in $HoFe_2$ might test the proposed models of indirect magnetic interactions and check the adequacy of theoretical calculations for this type of material.

## 2. Experimental

An alloy specimen, grown by Y. J. Bi and D. Fort of the School of Metallurgy and Materials, The University of Birmingham, England, using the Czochralski method (Bi *et al.*, 1991) was crushed into small pieces. A tiny

rectangular fragment selected for synchrotron X-ray diffraction measurements was bound by two {110}, two $\{\bar{1}10\}$ and two {001} faces. The sample dimensions were measured and the faces indexed using optical and scanning electron Electroscan E3 ESEM microscopes.

Diffraction intensities for $HoFe_2$ were measured at room temperature with 0.75 Å synchrotron X-radiation using the BL14A four-circle diffractometer (Satow & Iitaka, 1989) at the Photon Factory, Tsukuba. Vertically polarized X-radiation (polarization ratio ~0.95) from a vertical wiggler was monochromated by a double Si(111) perfect crystal monochromator and focused using a curved mirror. A high-speed avalanche photodiode (APD) detector with an intrinsic detection efficiency of 54.9% at 0.75 Å and a counting linearity up to $10^8$ c.p.s. was used (Kishimoto, 1995; Kishimoto *et al.*, 1998). The experimental setup was similar to that described by Streltsov *et al.* (1998).

Lattice constants were evaluated from the diffractometer setting angles for six symmetry-related (800) reflections at $2\theta = 48.46^\circ$. Reflection intensities were measured systematically using $\omega/2\theta$ continuous-time scans with a sampling time of 10 ms for a complete sphere of reciprocal space up to $(\sin\theta/\lambda)_{max} = 1.0945$ Å$^{-1}$. Intensities for six standard reflections, $(\pm800)$, $(0\pm80)$ and $(00\pm8)$, were remeasured periodically to monitor the incident beam stability. The measured intensities were normalized using the incident beam intensities monitored during each scan. The integrated intensities were further modified and structure-factor variances from counting statistics were adjusted for source instability as indicated by the standards (Rees, 1977). Further experimental details are listed in Table 1.†

Lorentz and polarization corrections were applied. Absorption correction factors (Alcock, 1974) were evaluated analytically using linear absorption coefficients at a wavelength of 0.75 Å evaluated from atomic absorption coefficients $\mu/\rho$ (cm$^2$ g$^{-1}$) of 79.2 for Ho and 42.6 for Fe calculated by Creagh (1996). The reference state for all structure-factor calculations was the independent-atom model (IAM) evaluated using spherical atomic scattering factors with dispersion corrections $\Delta f'$, $\Delta f''$ of $-0.251$ and 5.132 for Ho, and 0.353 and 0.935 for Fe at 0.75 Å calculated by Creagh (1996). The IAM model was favoured because it makes few prejudgments about the nature of the bonding in the $HoFe_2$ structure.

The calculations of the atomic absorption coefficients and the anomalous-dispersion corrections (Creagh, 1996) were based on techniques identical to those used in *International Tables for Crystallography* (1992, Vol. C). The $\mu/\rho$ and $\Delta f''$ values for the Ho and Fe atoms are very close to those evaluated by Sasaki (1989, 1990). However, Sasaki's values for the dispersion corrections $\Delta f'$ of $-0.699$ for Ho and 0.308 for Fe at 0.75 Å are

Table 1. *Experimental details*

| | |
|---|---|
| Crystal data | |
| Chemical formula | $HoFe_2$ |
| Chemical formula weight | 276.62 |
| Cell setting | Cubic |
| Space group | $Fd\bar{3}m$ |
| $a$ (Å) | 7.3091 (6) |
| $V$ (Å$^3$) | 390.5 (1) |
| $Z$ | 8 |
| $D_x$ (Mg m$^{-3}$) | 9.411 |
| Radiation type | X-ray vertical wiggler |
| Wavelength (Å) | 0.75 |
| No. of reflections for cell parameters | 6 |
| $\theta$ (°) | 24.23 |
| $\mu$ (mm$^{-1}$) | 60.63 |
| Temperature (K) | 293 |
| Crystal size (mm) | 0.018 × 0.016 × 0.0032 |
| Crystal colour | Black |
| | |
| Data collection | |
| Diffractometer | BL14A four-circle |
| Monochromator | Si(111) |
| Detector | APD |
| Data collection method | $\omega$–$2\theta$ scans |
| Scan speed (° min$^{-1}$) | 16 |
| Peak scan width $\omega$ (°) | 0.4 |
| Absorption correction | Analytical |
| $T_{min}$ | 0.433 |
| $T_{max}$ | 0.823 |
| No. of measured reflections | 3857 |
| No. of observed reflections | 3381 |
| Criterion for observed reflections | $I > 2\sigma(I)$ |
| No. of independent reflections | 116 |
| $R_{int}$ | 0.067 |
| $\theta_{max}$ (°) | 55.17 |
| Range of $h$, $k$, $l$ | $-16 \rightarrow h \rightarrow 16$<br>$-16 \rightarrow k \rightarrow 16$<br>$-16 \rightarrow l \rightarrow 16$ |
| No. of standard reflections | 6 |
| Frequency of standard reflections | Every 94 reflections |
| Intensity decay (%) | 3.7 |
| | |
| Refinement | |
| Refinement on | $F$ |
| $R$ | 0.00956 |
| $wR$ | 0.01098 |
| $S$ | 1.403 |
| No. of reflections used in refinement | 116 |
| No. of parameters used | 4 |
| Weighting scheme | $w = 1/\sigma^2(F)$ |
| $(\Delta/\sigma)_{max}$ | $< 0.001$ |
| $\Delta\rho_{max}$ (e Å$^{-3}$) | 1.58 |
| $\Delta\rho_{min}$ (e Å$^{-3}$) | $-0.70$ |
| $\sigma(\Delta\rho)$† (e Å$^{-3}$) | 0.20 |
| Extinction method | Maslen & Spadaccini (1993) |
| Extinction coefficient $r$* | 24 (36) |
| Extinction correction $y_{min}$ | 0.996 |
| Source of atomic scattering factors | *International Tables for Crystallography* (1992, Vol. C) |

† Mean s.u. value (Cruickshank, 1949).

† Supplementary data for this paper are available from the IUCr electronic archives (Reference: CR0535). Services for accessing these data are described at the back of the journal.

significantly different, especially for the Ho atom. When these values were included in the structural model refined by least squares, the scale factor was the only parameter which changed noticeably. The deformation electron density was virtually identical to that obtained with dispersion corrections calculated by Creagh (1996) and appears to be insensitive to variation of the $\Delta f'$ corrections.

Before refining structural parameters, an extinction correction for the full data set based on intensities for symmetry-equivalent reflections with different path lengths (Maslen & Spadaccini, 1993) was attempted. The minimum extinction correction $y_{\min}$ ($F_{\rm obs} = yF_{\rm kin}$, where $F_{\rm kin}$ is the value of the kinematic structure factor) applied was less than 0.5% for the $(0\bar{2}2)$ reflection. Symmetry-equivalent reflections were then averaged. Variances consistent with measurement statistics were retained. Those for the other reflections were increased according to the scatter of equivalents following a Fisher test.

The extinction parameter was also estimated as part of least-squares optimization of the structural model. The widely invoked formula of Zachariasen (1967) included in the refinement according to Larson (1970) yielded an $r^*$ extinction parameter which varied slightly within one s.u. The minimum extinction correction ($y_{\min}$) was 0.99. This is consistent with the estimation of extinction corrections by the comparison of equivalent reflections, increasing our confidence in the extinction-correction evaluation.

Four independent structural parameters, including the scale factor, one isotropic and two anisotropic elements of atomic displacement tensors for Ho and Fe, respectively, were refined by conventional full-matrix least squares including all observed structure factors. Further details of the data refinement are given in Table 1. These calculations were based on the *Xtal*3.4 system of crystallographic programs (Hall *et al.*, 1995) implemented on DEC ALPHA workstations.

The refinement of anharmonic atomic displacements was then attempted. The anharmonic displacements, represented by the cumulant expansion (*International Tables for Crystallography,* 1993, Vol. B) up to fourth rank, were included in least-squares optimization of the IAM model using the *VALRAY* program (Stewart & Spackman, 1983). Only one third-order coefficient, $c_{123}$, for the Ho atom and two fourth-order coefficients, $c_{1111}$ ($= c_{2222} = c_{3333}$) and $c_{1122}$ ($= c_{1133} = c_{2233}$), for each atom type are independent variables for the Ho ($\bar{4}3m$ symmetry) and Fe ($\bar{3}m$ symmetry) sites in the $HoFe_2$ structure. The fourth-order anharmonic terms are significantly less than one s.u. and only the $c_{123}$ (Ho) coefficient is of marginal significance in Table 2. Resulting atomic displacement tensors $U^{ij}$ and reliability factors were similar to those obtained for the harmonic model. The effect of anharmonicity on the $\Delta\rho$ was within the experimental error.

Table 2. *Fractional coordinates, harmonic $U^{ij}$ ($\AA^2$), third-order $c_{ijk}$ ($\times 10^7$ $\AA^3$) and fourth-order $c_{ijkl}$ ($\times 10^7$ $\AA^4$) anharmonic displacement parameters, and selected distances ($\AA$) with s.u.'s in parentheses for $HoFe_2$*

$$T = \exp[-2\pi^2 a^{-2} \sum U^{ij} h^i h^j] \exp[-i(4/3)\pi^3 a^{-3} \sum c_{ijk} h^i h^j h^k].$$

| | Ho | Fe |
|---|---|---|
| $x = y = z$ | 1/8 | 1/2 |
| $U^{11} = U^{22} = U^{33}$ | 0.00673 (2) | 0.00667 (4) |
| $U^{12} = U^{13} = U^{23}$ | 0 | 0.00012 (5) |
| $c_{123}$ | −54 (52) | 0 |
| $c_{1111} = c_{2222} = c_{3333}$ | 1.3 (50) | −0.4 (100) |
| $c_{1122} = c_{1133} = c_{2233}$ | −0.9 (110) | −0.6 (240) |
| | | |
| Ho–Ho$^{i}$ | | 3.1649 (2) |
| Ho–Fe$^{ii}$ | | 3.0302 (2) |
| Fe–Fe$^{ii}$ | | 2.5842 (2) |

Symmetry codes: (i) $-y, \frac{1}{4}+x, \frac{1}{4}+z$; (ii) $\frac{3}{4}-x, y, \frac{3}{4}-z$.

## 3. Results and discussion

### 3.1. *Structural and atomic displacement parameters*

The $HoFe_2$ structure with origin at the Ho-atom $\bar{4}3m$ site is depicted in Fig. 1. The Fe atoms are at the cubic $\bar{3}m$ positions. The positional and refined anharmonic displacement parameters with selected bond lengths are listed in Table 2. The $HoFe_2$ Laves crystal is characterized by the $MgCu_2$-type ($C15$) cubic structure. The structural parameters and deformation density distribution for $MgCu_2$ were studied by Ohba *et al.* (1984).

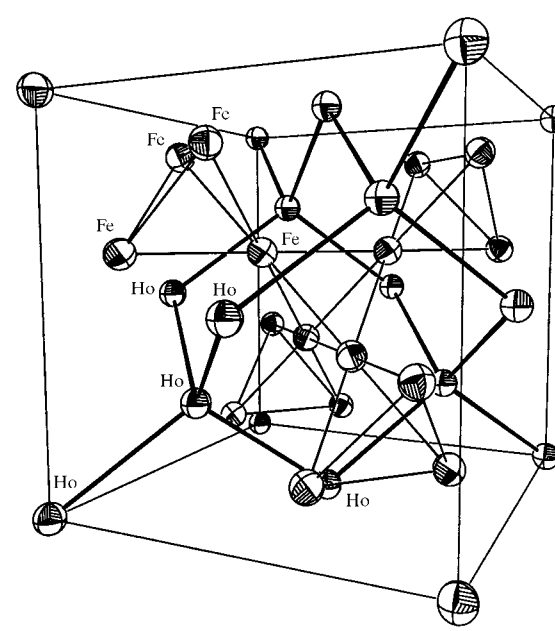


Fig. 1. The cubic unit cell of $HoFe_2$. Atomic displacement ellipsoids are shown at the 99% probability level.

The *C*15-type $HoFe_2$ structure is 'topologically' close-packed and is formed by three types of tetrahedra with common Fe–Fe edges. Every ideal $Fe_4$ tetrahedron shown in Fig. 1 is surrounded by four $HoFe_3$ and six $Ho_2Fe_2$ irregular tetrahedra. The Fe–Fe edges of the $Fe_4$ tetrahedra in Table 2 are less than the Fe–Fe contacts of 2.86645 (1) Å in crystalline $\alpha$-Fe metal. Projected onto the (111) plane, the $Fe_4$ tetrahedra form regular triangles and hexagons of the kagomé net, a detailed description of which was given by Ohba *et al.* (1984) for $MgCu_2$. The Ho atoms form a diamond-like sublattice shown by the thick bonds in Fig. 1. Each *R* atom is surrounded by twelve Fe atoms at distance of $a(11/8)^{1/2}$. The $HoFe_{12}$ polyhedra share common edges and hexagonal faces along the [111] directions.

Atomic displacement ellipsoids for $HoFe_2$ at the 99% probability level are depicted in Fig. 1. The anisotropy of the Fe-atom displacement is negligible. The diagonal terms of the Ho and Fe atomic displacement tensors are very similar. The small values of the anharmonic and harmonic atomic displacement parameters in Table 2 indicate that the $HoFe_2$ structure is stiff and tightly packed, as expected from the small Ho atomic radius. Metal–metal interactions should strongly affect the electron density distribution in such a tightly packed structure.

### 3.2. *Electron density*

Figs. 2(*a*), (*b*), (*c*) and (*d*) show the deformation density ($\Delta\rho$) sections in the (110) diagonal plane of the Ho–Ho and Fe–Fe contacts, in the (111) plane through the kagomé net marked with solid lines, in the $(1,1,\frac{1}{2})$ plane through the Ho–Fe contacts, and in the (001) plane through the Ho atoms, respectively. The $\Delta\rho$ maps were calculated including the anharmonic displacement parameters. The 0.25 e $Å^{-3}$ contour intervals are greater than the mean $\sigma(\Delta\rho)$ value listed in Table 1. The s.u.'s at points near special positions in the $\Delta\rho$ were derived according to equation (4) in the paper by Maslen (1988).

The $\Delta\rho$ map in Fig. 2(*a*) for $HoFe_2$ is remarkable for the large [1.5 (9) e $Å^{-3}$] accumulation of electron density between rare-earth metals. These features resemble the classical peaks attributed to 'covalent

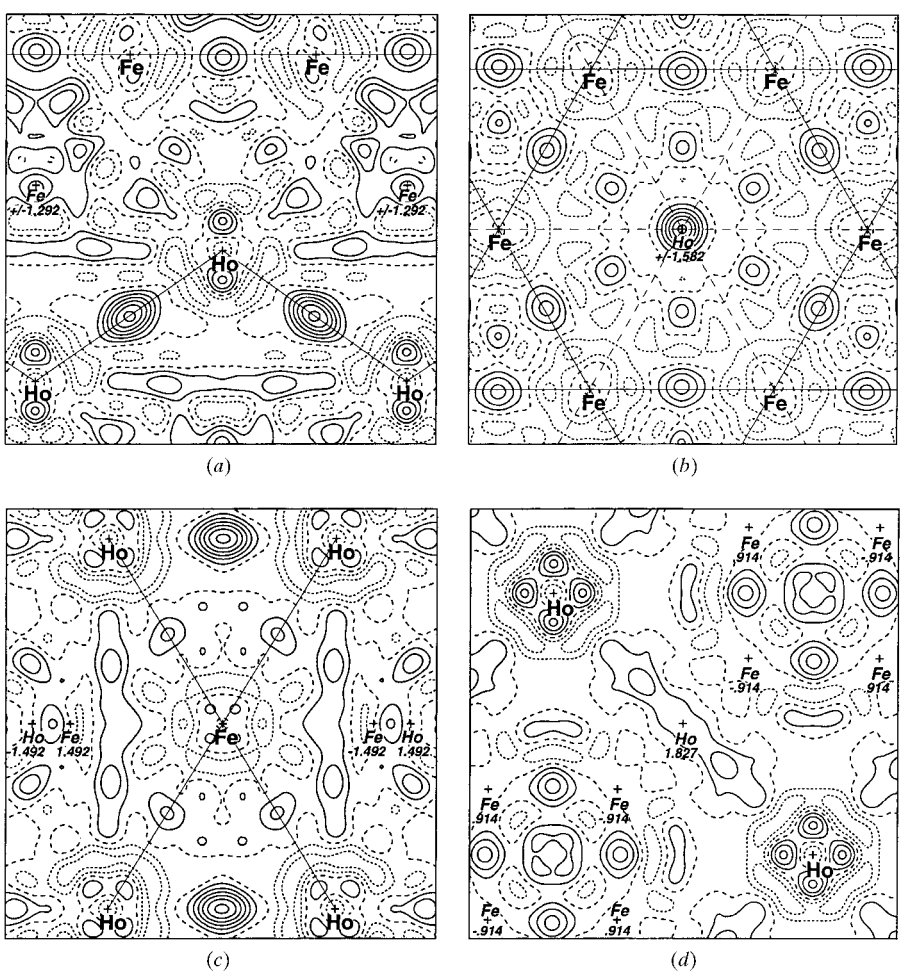


Fig. 2. $\Delta\rho$ maps for $HoFe_2$: (*a*) in the (110) diagonal plane, (*b*) in the (111) plane through the Fe atoms, (*c*) in the $(1,1,\frac{1}{2})$ plane through the Ho–Fe contacts and (*d*) in the (001) plane through the Ho atoms. Atoms deviating from the plane and their deviations are shown in italics. The map borders are 6.0 × 6.0 Å. Contour intervals are 0.25 e $Å^{-3}$; positive contours are solid and negative contours are shown as short-dashed lines.

bonding' in silicon and diamond crystals (see *e.g.* Lu & Zunger, 1992; Yamanaka & Morimoto, 1996). The cross section of the excess electron density midway between the Ho atoms is shown at the centre of the map in Fig. 2(*b*). The distance of 1.58 Å from this peak to the Ho atoms is less than the Ho metallic radius of 1.77 Å (Alcock, 1990). These residual electrons accumulate at the centres of the kagomé hexagons and form, with the Fe atoms, a triangular lattice marked with broken lines in Fig. 2(*b*). Such an electronic arrangement may be relevant to the atomic and magnetic structure stability in cubic Laves compounds. There are certain atomic configurations in solids where the interaction between individual electron spins is strong but highly competitive. These are unstable in the sense that the neighbouring spins demand conflicting orientation for a specific spin, promoting dynamic fluctuations of the magnetic moments (spins). As theoretical calculations by Leung & Elser (1993) and Leung & Runge (1993) showed, the kagomé net is an example where the geometrical 'frustration' alone can create a magnetically disordered ground state, in contrast to the triangle lattice where the ground state is believed to have magnetic order.

High sixfold symmetry of the $\Delta\rho$ around the centre of the kagomé hexagon in Fig. 2(*b*) reflects the geometry of the nearest Fe atoms in the plane perpendicular to the threefold crystallographic axis. Figs. 2(*a*) and (*b*) also contain accumulations of electron density between the Fe atoms. These excess-electron-density regions have similar shapes to those between the Ho atoms in Fig. 2(*a*) and maximum values of 0.8 (3) e Å$^{-3}$ at the midpoints of the Fe–Fe contacts, which are shorter than the Fe–Fe distances in crystalline $\alpha$-Fe. It is interesting to note that the $\Delta\rho$ around the Ho and Fe atoms (Figs. 2*a* and *c*) also have similar shapes, reflecting strong Ho–Fe interactions. A high degree of correlation between aspherical electron densities around rare-earth and Fe atoms was observed by Streltsov & Ishizawa (1999) in magnetic $R$FeO$_3$ perovskite orthoferrites.

Positive $\Delta\rho$ accumulates slightly near the Fe nucleus, whereas the depleted regions are further away, as shown in Figs. 2 (*a*)–(*c*). In Fig. 2(*c*) the depleted $\Delta\rho$ region near the Fe atom is surrounded by a belt of positive peaks including those of ~0.5 (2) e Å$^{-3}$ at the midpoint between the Ho and Fe atoms. The 'covalent' interactions between the Ho and Fe atoms were confirmed by *ab initio* density-functional calculations for HoFe$_2$ (Brooks, 1991).

Nevertheless, theoretical calculations were unable to predict the Ho–Ho 5*d*–5*d*-type orbital interactions strongly indicated by the $\Delta\rho$ map in Fig. 2(*a*). The accumulation of charge density between the Ho–Ho, Fe–Fe and Ho–Fe atoms is relevant to the model proposed by Campbell (1972) of the magnetic interactions due to 3*d*–3*d*, 5*d*–3*d* and 5*d*–5*d* orbital mixing. The 5*d* electrons are far less localized than the 4*f* electrons, and considerable overlap occurs between the rare-earth 5*d* wave functions and the 5*d*/3*d* wave functions of neighbouring atoms.

A small area of depleted electron density at the Ho site is surrounded by six lobes of positive density with a maximum of 0.75 (2) e Å$^{-3}$ at ~0.38 Å from the nucleus in Figs. 2(*a*) and (*d*). As the rare-earth 4*f* electron subshells are characterized by a radius of ~0.35 Å, these peaks can be attributed to the aspherical electron density distribution of the Ho 4*f* electrons. The optical criterion for the resolution of the electron-density Fourier series (James, 1982) suggests that details of the electron density on a larger scale than $r = 0.61/(2\sin\theta/\lambda)_{\max} = 0.28$ Å can be resolved. Moreover, similar features of the electron density near the cubic symmetry sites of the rare-earth metals were recently observed by Tanaka *et al.* (1997) in $CeB_6$ and by Streltsov *et al.* (1997) in $SmB_6$.

The $\Delta\rho$ near the Mg atom in $MgCu_2$ (Ohba *et al.*, 1984) also exhibits aspherical deformations with a maximum at a distance of ~0.34 Å from the Mg nucleus. This distance is within the range ~0.3–0.38 Å of the characteristic radii for the 2*p*, 3*p* and 3*d* subshells. As the metallic Mg atom has filled *s* and *p* subshells, one might expect that the electron density surrounding Mg should remain spherically symmetric in $MgCu_2$. However, the overlap of the valence electrons with the closed inner subshells of neighbouring atoms alters the energies of the orbitals through exchange repulsion. The corresponding modification of the electron density is also field-dependent. Thus the most significant contribution to polarization of the electron density does not depend on the symmetry of the prepared state, but depends on the strength and geometry of the perturbing field.

Significant accumulations of the electron density are observed at the centres of the $Fe_4$ tetrahedra in Figs. 2(*a*) and (*d*). However, there is significantly less residual density at the centres of the $HoFe_3$ and $Ho_2Fe_2$ irregular tetrahedra (Figs. 2*a* and *b*). The residual electron density was also found only at the centres of the $Cu_4$ tetrahedra in $MgCu_2$ (Ohba *et al.*, 1984). Although this was not mentioned by Ohba *et al.*, the $\Delta\rho$ maps for $MgCu_2$ show excess electron density of ~0.2 and ~0.1 e Å$^{-3}$ midway along the Mg–Mg and Cu–Cu contacts, respectively. However, without knowing the s.u.'s in the $\Delta\rho$ it is difficult to estimate the significance of these peaks in $MgCu_2$. The topography of the $\Delta\rho$ map in the (111) plane through the kagomé net formed by the Cu atoms in $MgCu_2$ resembles that in $HoFe_2$ shown in Fig. 2(*b*).

Although the main characteristics of the deformation density for magnetic $HoFe_2$ are similar to those of diamagnetic $MgCu_2$, the features in the $\Delta\rho$ maps discussed above are much more pronounced for $HoFe_2$. In particular, there are no strongly depleted regions around the Mg and Cu atoms in $MgCu_2$. However, the $\Delta\rho$ distribution is significantly depleted nearer the

nuclei along the Ho–Ho, Ho–Fe and Fe–Fe vectors in Fig. 2, at about the distances from the nuclei where the Ho 4*f*/5*d* and the Fe 3*d* subshells reach a maximum. These depletions are characteristic of exchange repulsion.

Although the features of the residual density concentrated near the Mg atom in $MgCu_2$ (Ohba *et al.*, 1984) are consistent with that expected from orbital populations and exchange interactions, it is possible that they could arise from anharmonic components in the thermal motion, not allowed for in the structural model of $MgCu_2$. For $HoFe_2$, the anharmonic refinement resulted in a slight (less than one s.u.) redistribution of the $\Delta\rho$ near the Ho and Fe atoms at distances of ~0.2 Å from the nuclei. For example, small $\Delta\rho$ lobes of $\pm 0.1$ (3) e Å$^{-3}$ near Ho in the [111] directions, which result from the dominating third-order anharmonic $c_{123}$ term, disappeared in the $\Delta\rho$ maps calculated with 0.1 e Å$^{-3}$ contour intervals including the anharmonic displacement parameters. This effect was almost unnoticeable in the maps calculated with 0.25 e Å$^{-3}$ contour intervals. Therefore, the features of the electron density near the Ho atom at a distance of 0.38 Å and, especially, those midway between the Ho atoms at a distance of 1.58 Å from Ho are mainly electronic in origin.

Thus, a synchrotron X-ray diffraction analysis of the deformation electron density for the intermetallic $HoFe_2$ Laves compound showed significant excess electron density midway along the Fe–Fe, the Ho–Fe and, particularly, the Ho–Ho contacts. This points to a model of magnetic interactions involving an ordinary 4*f*–5*d* exchange combined with the direct 3*d*–3*d*, 3*d*–5*d* and 5*d*–5*d* interactions and confirms the hypothesis that 5*d*-like electrons of the rare-earth atoms play an important role in the spin-coupling mechanism and magnetic properties of $HoFe_2$-type compounds. This result should also provide further support for the existence of 5*d*-like components of electron density associated with the diffuse magnetization in $HoFe_2$ (Zukowski *et al.*, 1993; Cooper *et al.*, 1993).

VAS wishes to thank Dr S. P. Collins (Daresbury Laboratory) for providing the crystalline material and to acknowledge valuable comments by the late Dr E. N. Maslen in the early stages of this work. This work was supported by the Australian Research Council. Financial support from the Australian Synchrotron Research Program funded by the Commonwealth of Australia *via* the Major National Research Facilities Program is also acknowledged.

## References

Alcock, N. W. (1974). *Acta Cryst.* A**30**, 332–335.
Alcock, N. W. (1990). *Bonding and Structure: Structure Principles in Inorganic and Organic Chemistry*. New York: Ellis Horwood.
Bi, Y. J., Abell, J. S. & Hwang, A. M. H. (1991). *J. Magn. Magn. Mater.* **99**, 159–166.
Brooks, M. S. S. (1991). *J. Appl. Phys.* **69**, 5683–5684.
Brooks, M. S. S., Nordström, L. & Johansson, B. (1991). *J. Phys. Condens. Matter*, **3**, 2357–2371.
Campbell, I. A. (1972). *J. Phys. F: Metal Phys.* **2**, L47–L50.
Cooper, M. J., Zukowski, E., Timms, D. N., Armstrong, R., Itoh, F., Tanaka, Y., Ito, M., Kawata, H. & Bateson, R. (1993). *Phys. Rev. Lett.* **71**, 1095–1098.
Creagh, D. C. (1996). Private communication.
Cruickshank, D. W. J. (1949). *Acta Cryst.* **2**, 65–82.
Gignoux, D. & Schmitt, D. (1995). *Magnetic Properties of Intermetallic Compounds. Handbook on the Physics and Chemistry of Rare Earths*, Vol. 20, edited by K. A. Gschneider Jr and L. Eyring, pp. 293–424. Amsterdam: Elsevier Science BV.
Hall, S. R., King, G. S. D. & Stewart, J. M. (1995). *Xtal3.4 Reference Manual.* University of Western Australia, Australia.
James, R. W. (1982). *The Optical Principles of the Diffraction of X-rays.* Woodbridge, Connecticut: Ox Bow Press.
Kishimoto, S. (1995). *Rev. Sci. Instrum.* **66**, 2314–2316.
Kishimoto, S., Ishizawa, N. & Vaalsta, T. P. (1998). *Rev. Sci. Instrum.* **69**, 384–391.
Larson, A. C. (1970). *Crystallographic Computing*, edited by F. R. Ahmed, S. R. Hall and C. P. Huber, pp. 291–294. Copenhagen: Munksgaard.
Leung, P. W. & Elser, V. (1993). *Phys. Rev. B*, **47**, 5459–5462.
Leung, P. W. & Runge, K. J. (1993). *Phys. Rev. B*, **47**, 5861–5873.
Lu, Z. W. & Zunger, A. (1992). *Acta Cryst.* A**48**, 545–554.
Maslen, E. N. (1988). *Acta Cryst.* A**44**, 33–37.
Maslen, E. N. & Spadaccini, N. (1993). *Acta Cryst.* A**49**, 661–667.
Ohba, T., Kitano, Y. & Komura, Y. (1984). *Acta Cryst.* C**40**, 1–5.
Rees, B. (1977). *Isr. J. Chem.* **16**, 180–186.
Sasaki, S. (1989). *Numerical Tables of Anomalous Scattering Factors Calculated by the Cromer and Mann's Method.* KEK Report 88-14, 1-136. Photon Factory, Tsukuba, Japan.
Sasaki, S. (1990). *X-ray Absorption Coefficients for the Elements (Li to Bi, U).* KEK Report 90-16, 1-143. Photon Factory, Tsukuba, Japan.
Satow, Y. & Iitaka, Y. (1989). *Rev. Sci. Instrum.* **60**, 2390–2393.
Stewart, R. F. & Spackman, M. A. (1983). *VALRAY User's Manual.* Carnegie–Mellon University, Pittsburg, USA.
Streltsov, V. A. & Ishizawa, N. (1999). *Acta Cryst.* B**55**, 1–7.
Streltsov, V. A., Ishizawa, N. & Kishimoto, S. (1998). *J. Synchrotron Rad.* **5**, 1309–1316.
Streltsov, V. A., Maslen, E. N. & Ishizawa, N. (1997). *Photon Factory Activity Report* 1996. KEK Progress Report 97-2 A/M. Vol. 14, p. 305. High Energy Accelerator Research Organization, Photon Factory, Tsukuba, Japan.
Tanaka, K., Kato, Y. & Ōnuki, Y. (1997). *Acta Cryst.* B**53**, 143–152.
Yamanaka, T. & Morimoto, S. (1996). *Acta Cryst.* B**52**, 232–238.
Zachariasen, W. H. (1967). *Acta Cryst.* **23**, 558–564.
Zukowski, E., Collins, S. P., Cooper, M. J., Timms, D. N., Itoh, F., Sakurai, H., Kawata, H., Tanaka, Y. & Malinowski, A. (1993). *J. Phys. Condens. Matter*, **5**, 4077–4090.